Journal of Applied Meteorology and Climatology

GSI-BASED HYBRID 3DVAR DATA ASSIMILATION FOR THE BAM-CPTEC/INPE: SINGLE LOW RESOLUTION EXPERIMENTS

--Manuscript Draft--

Manuscript Number:	
Full Title:	GSI-BASED HYBRID 3DVAR DATA ASSIMILATION FOR THE BAM-CPTEC/INPE: SINGLE LOW RESOLUTION EXPERIMENTS
Article Type:	Article
Corresponding Author:	Carlos Frederico Bastarz, Msc. INPE Cachoeira Paulista, Sao Paulo BRAZIL
Corresponding Author's Institution:	INPE
First Author:	Carlos Frederico Bastarz, Msc.
Order of Authors:	Carlos Frederico Bastarz, Msc.
	Dirceu Herdies
Manuscript Classifications:	8.052: Data assimilation; 8.148: Numerical weather prediction/forecasting
Abstract:	This paper aims to present the first results obtained with a GSI-based Hybrid Ensemble-Variational system applied to the Brazilian Atmospheric Model from Center for Weather Forecasts and Climate Studies at the National Institute for Space Research (BAM-CPTEC/INPE). The hybrid data assimilation system implemented is a hybrid 3DVar, using the Ensemble Kalman Filter (EnKF) and the Gridpoint Statistical Interpolation (GSI) 3DVar analysis system. This is an upgrade to the previous GSI 3DVar system being used at CPTEC operations. The implementation was made using a previous established model and assimilation framework. A new background error covariance matrix was calculated, in order to properly account the ensemble covariance contribution to the static climatological part. An analysis and an evaluation of the updated system is presented and the first results for analyses and 5-day forecasts at TQ0062L028 model resolution are presented as well. The tested hybrid 3DVar system at CPTEC shows an improvement for the BAM-CPTEC/INPE skill mainly over South America and Tropical region and endorses the use of ensemble covariances as a complement to the static part of the covariances as a way to reduce the misrepresentation of the background error covariances. Precipitation has been also evaluated in a comparison with observed data. Exercising with the hybrid system have shown an improvement over the pure 3DVar system in both the intensity and the distribution of the precipitation over the time mean. The results obtained with the implementation are encouraging and further improvements must be made in order to fully access the analysis and forecast skill, specially under higher resolutions.
Suggested Reviewers:	Jeffrey Whitaker jeffrey.s.whitaker@noaa.gov Jeffrey Whitaker work refers to ensemble Kalman filters and hybrid methods in data assimilation.
	Daryl Kleist daryl.kleist@noaa.gov Daryl Kleist work refers to the Gridpoint Statistical Interpolation system and hybrid methods in data assimilation.

Powered by Editorial Manager® and ProduXion Manager® from Aries Systems Corporation

Cover Letter
Click here to download Cover Letter
cover_letter_JAMC_bastarz_herdies_2017.pdf

Carlos Frederico Bastarz
National Institute for Space Research
Avenida dos Astronautas, 1778
Jardim da Granja
CEP 12227-010
São José dos Campos/SP Brazil

June 17, 2017

Dr. David Kristovich
Chief Editor of the Journal of Applied Meteorology and Climatology

We wish to submit a new manuscript entitled "**GSI-BASED HYBRID 3DVAR DATA ASSIMILATION FOR THE BAM-CPTEC/INPE: SINGLE LOW RESOLUTION EXPERIMENTS**" for consideration by the Journal of Applied Meteorology and Climatology.

This research is related to the application of a GSI-based hybrid 3DVar data assimilation coupled to the CPTEC/INPE general circulation model. The objetive of this research is to verify the impacts of the use of ensemble Kalman filter covariances combined with static covariances. This static covariance matrix was calculated using 730 pairs of 48/24 hours forecasts. The hybrid 3DVar system, is exercised with 40 members and a real non linear model. The results are encouraging and shows that when using the hybrid covariances with a greater contribution from the ensemble part, the forecasts skill are improved for various model state variables. We also show that hybrid covariances can also help the model to improve the distribution of the 24 hour precipitation, in both space and time. As we have evaluated the system performance for different regions of the globe, we found that the ensemble covariances helped the model to improve its skill in regions that are known to have a lower conventional observation coverage (eg. South Hemisphere/South America). We believe that this results whould be of the interest of the journal readers because it endorses the use of hybrid covariances in data assimilation applications, specially over the southern hemisphere.

We confirm that this work is original and has not been published elsewhere nor is it currently under consideration for publication elsewhere. All authors have approved the manuscript and agree with its submission to the Journal of Applied Meteorology and Climatology.

Please address all correspondence concerning this manuscript to me at carlos.frederico@cptec.inpe.br.

Thank you for your consideration of this manuscript.

Sincerely,

Carlos Frederico Bastarz on behalf of the authors

Click here to access/download
Cost Estimation and Agreement Worksheet
Cost Estimation and Agreement Worksheet_FILL.pdf

LaTeX File (.tex, .sty, .cls, .bst, .bib) Click here to download LaTeX File (.tex, .sty, .cls, .bst, .bib) amssamp1.tex

GSI-BASED HYBRID 3DVAR DATA ASSIMILATION FOR THE BAM-CPTEC/INPE: SINGLE LOW RESOLUTION EXPERIMENTS

Carlos Frederico Bastarz* and Dirceu Luis Herdies †

Center for Weather Forecast and Climate Studies, CPTEC/INPE, Cachoeira Paulista, SP, Brazil

Corresponding author address: Carlos Frederico Bastarz, CPTEC/INPE, Rod. Presidente Dutra, km 40, Cachoeira Paulista, SP, Brazil.

E-mail: carlos.frederico@cptec.inpe.br

†Center for Weather Forecast and Climate Studies, CPTEC/INPE, Cachoeira Paulista, SP, Brazil

ABSTRACT

This paper aims to present the first results obtained with a GSI-based Hybrid Ensemble-Variational system applied to the Brazilian Atmospheric Model from Center for Weather Forecasts and Climate Studies at the National Institute for Space Research (BAM-CPTEC/INPE). The hybrid data assimilation system implemented is a hybrid 3DVar, using the Ensemble Kalman Filter (EnKF) and the Gridpoint Statistical Interpolation (GSI) 3DVar analysis system. This is an upgrade to the previous GSI 3DVar system being used at CPTEC operations. The implementation was made using a previous established model and assimilation framework. A new background error covariance matrix was calculated, in order to properly account the ensemble covariance contribution to the static climatological part. An analysis and an evaluation of the updated system is presented and the first results for analyses and 5-day forecasts at TQ0062L028 model resolution are presented as well. The tested hybrid 3DVar system at CPTEC shows an improvement for the BAM-CPTEC/INPE skill mainly over South America and Tropical region and endorses the use of ensemble covariances as a complement to the static part of the covariances as a way to reduce the misrepresentation of the background error covariances. Precipitation has been also evaluated in a comparison with observed data. Exercising with the hybrid system have shown an improvement over the pure 3DVar system in both the intensity and the distribution of the precipitation over the time mean. The results obtained with the implementation are encouraging and further improvements must be made in order to fully access the analysis and forecast skill, specially under higher resolutions.

1. Introduction

Hybrid data assimilation systems using an ensemble Kalman Filter and a variational technique have been developed (e.g., Hamill and Snyder 2000; Lorenc 2003; Zupanski 2005) and applied focusing the sampling and the representation of the spatial-temporal variations of background error covariances, introducing the day-to-day statistics variations of the background flow (the so called "errors of the day" - Corazza et al. 2003) to the static part of the variational covariances. The representation of background error covariances is one of the main issues of the operational data assimilation and its specification for deterministic systems (e.g., variational systems) is of a primordial importance.

Variational systems such as 3DVar uses a static background error covariance matrix, which means that its covariances are stationary in time and does not vary, thus the same error statistics are used for the whole assimilation process. A similar situation happens to a 4DVar system, which - in general, uses a pre-computed covariance background error matrix at the beginning of each assimilation window, which is at least propagated in time during the assimilation of observations using the tangent linear version of the forecast model. Differences in the way that background error statistics varies with time due to the variations in the background flow, leads to what we call flow-dependence.

Flow-dependent covariances are a key feature of modern data assimilation systems, and its specification either at the beginning or during the assimilation window, allows the analysis to correct account for the time and spatial dependency of the observation innovations being used into the analysis increments, in both horizontal and vertical directions. Furthermore, desirable features of the background error covariances also include anisotropy and inhomogeneity (non-uniform statistics - Rabier 2005).

Several efforts have been made in order to add some degree of flow-dependence and anisotropy to static covariances. The development of the variational techniques for operational use during the 1990's, include some sort of implicit modifications to the data assimilation framework. Desroziers (1997) introduced a coordinate transformation to allow the data assimilation system to better account for structures of frontal systems. This led to an improved analysis with flow dependent covariances and anisotropic correlations.

The gradients represented in the background flow, also include important information that could be used to allow anisotropy. Riishøjgaard (1998) showed how to use the humidity field to model correlation functions that can be stretched to accommodate the covariances according to the gradients represented in the background flow. Other approaches to model correlation functions that lead to flow-dependent background error statistics, involve the use of wavelets with spectral methods (e.g., Fisher 2003), but difficulties arise with the specification of these wavelets on the sphere. Recursive filters are also another know method to derive quasi-Gaussian shapes to use in background error covariance modeling. This approach have been used successfully in several applications; e.g., Hayden and Purser (1995) applied isotropic recursive filters to the processing of the National Environmental Satellite and Data Information Service (NESDIS); more recently, recursive filters have been applied to the Gridpoint Statistical Interpolation (GSI) to model the application of background error covariances (Wu et al. 2002).

Within these efforts, other approaches have been developed and are more related to the representation of nonlinearities of the background flow into the background error statistics. The 4DVar (Thpaut and Courtier 1991) was developed as an extension of 3DVar (Lorenc 1986) and can implicit evolve covariances inside the assimilation window. Corazza et al. (2003) added flow-dependence to covariances by accounting for the "errors of the day", using bred-vectors. Hybrid methods (e.g., Hamill and Snyder 2000) were introduced taking advantage of the ensemble Kalman Filter meth-

ods. This new approach has several advantages including the fact that operational centers have already experienced the variational technique and have some experience with ensemble Kalman Filters. Each of these methods can be taken as a compliment to ameliorate the deficiencies of the other (Wang et al. 2007, 2009). Recently, hybrid methods with real applications have been deployed (e.g., Wang et al. 2013; Clayton et al. 2013) where covariances estimated from an ensemble Kalman Filter, are linearly combined to a 3DVar static covariances matrix.

Most recent developments at CPTEC have focused on its independence on observations preprocessing, quality control and analysis. In the past few years, some analysis systems have been tested at CPTEC, including the GSI. GSI have been used in several operational NWP centers and is the data assimilation chosen for regional and global applications at the center.

With the objective of provide the BAM-CPTEC/INPE model (Figueroa et al. 2016) with its own analysis in a data assimilation cycle, in this paper are described the details of the implemented system and the first results obtained with the GSI-based hybrid 3DVar system.

This paper is organized as follows: Section 2 describes the strategy and the details of the implemented hybrid 3DVar system and the static part of the background error covariance matrix; Section 3 presents a description of the idealized experiments to test the hybrid system. Results from the experiments carried out are represented in Section 4 and finally, Section 5 presents the discussion regarding the results and future plans.

2. CPTEC Global Hybrid 3DVar System

In the past years, hybrid data assimilation systems have shown an increasing amount of development and several centers have been made efforts to take advantage of its benefits. Hybrids systems using the 3DVar and an ensemble Kalman Filter (EnKF) appears to be a common choice to start with. The GSI system comprises a collection of routines that are already prepared to run such

a hybrid 3DVar system using the EnKF to provide the ensemble covariances to compliment the static covariances used in 3DVar.

Since 2012 CPTEC have been experimenting the GSI 3DVar analysis with its global General Circulation Model (GCM) for NWP until 7 days at a TQ0299L064 spectral model resolution (roughly, 45 km at the Equator, with a corresponding grid of 450 X 900 X 64 points, *lat* X *lon* X *lev*). This version of the system was performed with a GSI's example global background error covariance matrix (with a grid of 386 X 768 X 64 points, *lat* X *lon* X *lev*). Although this configuration seems to be not the ideal, it was a first attempt to run a global analysis with radiance data assimilation at a higher resolution at CPTEC.

With the public release of the hybrid version of GSI in 2015, CPTEC started to plan a revamped version of its global data assimilation system. A new version of the BAM-CPTEC/INPE model was released in the summer of 2015 and was planned a test of running the BAM-CPTEC/INPE with its own analysis, but using a proper background error covariance matrix and also testing with the new hybrid system structure of GSI.

Exercise with the hybrid 3DVar assimilation technique with the BAM-CPTEC/INPE, was made using the Ensemble Square Root Filter (EnSRF - Whitaker and Hammill 2002). Two experiments were carried out: one experiment using 50% of ensemble contribution to the static covariance and a second experiment with 75% of ensemble contribution, were designed to test the hybrid 3DVar system. Another experiment with a pure 3DVar using the BAM-CPTEC/INPE in a cycled data assimilation and the realization of the BAM-CPTEC/INPE with the National Centers for Environmental Predictions (NCEP) analysis were also performed. For the three experiments using data assimilation, the new static version of the background error covariance matrix were used. As we have made a new background error covariance matrix for use in the experiments with the traditional 3DVar and the hybrid data assimilation, Subsection 2a shows the details and main aspects

the the new static matrix. Subsections 2b and 2c are dedicated to present the BAM-CPTEC/INPE model information and the main setup for the hybrid 3DVar system, respectively. A detailed description of the experiments is given in Section 3.

a. Static Background Error Covariance Matrix

The background error covariance matrix (**B**) has the role to filter and propagate spatially the observation information (Berre et al. 2013), contributing to transform part of the observations innovations into analysis increments.

The calculation of the background error covariance matrix for the GSI system used in this work, involved the use of 730 pairs of 48 and 24 hours forecasts, valid for the 0000 and 1200UTC, distributed evenly over 1 year (2013). The resolution of the forecasts matches the resolution of the forecast model used in the experiments, i.e., TQ0062L028 (with 192 x 96 x 28 - *lat* X *lon* X *lev* grid points). The forecasts pairs were organized as follows: considering 2014010100, the first valid forecast pair was generated with the analysis from 2013123100 (valid for a 24 hours forecast) and 2013123000 (valid for a 48 hours forecast). The methodology used to calculate the amplitudes (i.e., the variances and covariances) is based on the NMC method (Parrish and Derber 1992). This method claims that spatial correlations of the model errors are similar to the spatial correlations of the differences between the 48 and 24 hours forecasts. The NMC method was chosen for the background error covariance calculations due to the convenience of having previously analyses from operations. These analyses were used to integrate the BAM-CPTEC/INPE model at TQ0062L028 resolution for one year. Within the algorithm involved in the calculations, there is also a procedure to remove the bias in the vertical model column, which were also used. Covariances were calculated for the standard GSI control variables, i.e., streamfunction (ψ), unbalanced velocity potential (χ), unbalanced temperature (T), unbalanced surface pressure (ps) and the nor-

malized relative humidity (*rh*). The sea surface temperature (*sst*) is the same as the one used on the GFS-NCEP background error covariance matrix (i.e., the Real-Time, Global, Sea Surface Temperature - RTG_SST analysis, from which the variances and length scales were interpolated to the target grid).

In practice, although GSI doesn't explicit construct **B**, it applies the covariances of **B** using recursive filters (Purser et al. 2003a,b):

$$\mathbf{B} = \mathbf{B}_z(V^1\mathbf{B}_x^1\mathbf{B}_y^1\mathbf{B}_y^1\mathbf{B}_x^1V^1 + V^2\mathbf{B}_x^2\mathbf{B}_y^2\mathbf{B}_y^2\mathbf{B}_x^2V^2)\mathbf{B}_z \tag{1}$$

where,

- V^1 and V^2 are the standard deviations of each control variable (from the **B** file);
- $\mathbf{B}_x$, $\mathbf{B}_y$ and $\mathbf{B}_z$ are the recursive filter applications in the directions of x (west-east), y (south-north) and z (vertical);
- $\mathbf{B}^1$ and $\mathbf{B}^2$ represents the application of the recursive filter in the horizontal scales (x and y).

An important property of the recursive filters in the GSI framework, is the adjustment of the amplitudes and the length scales in order to make the aspect of the covariances anisotropic, letting them to adjust to the background flow. These parameters and scales used in the application of the recursive filters are sort of empirical and a discussion of it can be found in Wu et al. (2002). The resulting amplitudes of the calculated **B** are presented in Section 4a.

b. The Brazilian Atmospheric Model (BAM)

CPTEC has been made efforts to continuously develop and improve its own GCM for operational use at the center. As a result of this efforts, the BAM-CPTEC/INPE (Figueroa et al. 2016) brings

the most recent advances in both model dynamics and physics. Although the version of the BAM-CPTEC/INPE model used in this work is not exactly the same version used in Figueroa et al. (2016), the version used in the experiments will be referred as "BAM v0.0", which includes the same dynamical core and a simplified physics package (mostly described in Cavalcanti et al. 2002). This simplified physics package is based on a large scale condensation due to the chosen model resolution (TQ0062L028, roughly 200 km at the Equator) and the ensemble size (40 plus 1 of the hybrid analysis). Furthermore, microphysics was avoided due to the intense computational requirements (Silvio N. Figueroa, personal communication).

The BAM-CPTEC/INPE is a spectral model representing mass and winds in terms of vorticity and divergence, with a pure sigma vertical coordinate, used at the center for operational NWP (current resolution is TQ0666L064, roughly 20 km at the Equator) up to 5 days, and - at a coarse resolution (TQ0126L028, roughly 100 km near the Equator) for extended NWP up to 15 days, using an ensemble prediction system based on Empirical Orthogonal Functions (EOF) for the perturbation of the initial condition. Seasonal and climate simulations are made as well. For these applications analysis are still taken from GFS-NCEP.

c. Hybrid Ensemble-Variational Analysis Cycle

The hybrid 3DVar is the variational system with hybrid covariances intended to be the next generation of atmospheric analysis at CPTEC. This system was exercised in an experimental basis at CPTEC for weather forecasts only (up to 5 days at TQ0062L028 model resolution). Plans include to use the ensemble of analysis from the hybrid system to replace or to augment the current size (15 members) and consequently the spread of the center's global Ensemble Prediction System (EPS, described in Mendonça and Bonatti 2009; Cunningham et al. 2015), for extended atmospheric forecasts (up to 15 days). The hybrid system used in this work is coupled with the

BAMv0 model through an interface that reads the spectral forecasts from the BAMv0 model and rewrites the spectral coefficients for use as a background for the GSI system.

The current hybrid setup requires the realization of the GSI observer using the mean ensemble as a background. No analysis is made at this point and this step is only necessary to write the diagnostics files from the departures. The next step is the realization of the observer using the departures related to the ensemble mean, but using every ensemble member as a background. In the setup tested, an ensemble of 40 members was used. This number represents a reasonable ensemble size, which fits all the computational requirements, regarding the allowed computational time and disk space without compromise the efficiency. Once the observer ensemble of departures is computed within GSI, the EnSRF is applied to update the ensemble of backgrounds. The final deterministic hybrid 3DVar analysis is then achieved using the covariances from the updated ensemble of backgrounds, which are blended with the static pre-computed background error covariance matrix. Figure 1 shows a schematic diagram of the analysis cycle.

The hybrid 3DVar system minimizes a 3D variational cost function in the same fashion as 3DVar. The main difference is regarded to the way the background error covariance matrix is defined and applied. Equation 2 (presented here in a more general way) represents the hybrid 3DVar cost function, where x' is the new analysis increment.

$$J(x') = \frac{1}{2}(x')^T(\alpha_1\mathbf{B} + \alpha_2\mathbf{P}^b)^{-1}(x') + \frac{1}{2}[y_o - \mathbf{H}(x')]^T\mathbf{R}^{-1}[y_o - \mathbf{H}(x')] \quad (2)$$

Note that the term $(\alpha_1\mathbf{B} + \alpha_2\mathbf{P}^b)$ represents the linear combination between the pre-computed static $\mathbf{B}$ and the ensemble flow-dependend ensemble covariances $\mathbf{P}^b$. The coefficients α_1 and α_2 are the weights assigned to each parcel of the linear combination, trough which we control the amount of contribution of the ensemble covariances to the static part.

In Equation 2, x' is defined as:

$$x' = x + \sum_{k=1}^{K} (a_k \circ x_k^e) \tag{3}$$

This analysis increment is defined as the sum between the standard analysis increment (x) due to the static background error covariance contribution and the summing between the extension of the control variable (a_k, to account for the ensemble localization) and the ensemble perturbation of each member ($x_k^e = \frac{(x_k^b - \bar{x}^b)}{\sqrt{K-1}}$). A more detailed explanation of the GSI methodology to extend the variational framework to accommodate the ensemble covariances can be found in Wang et al. (2007, 2008a,b); Wang (2010); Wang et al. (2013).

Despite the fact that the hybrid 3DVar analysis cycle have been established for the BAMv0 model, some caveats have been found and will demand attention on future revisions of this system. The system works in a single resolution, i.e., both the control and the ensemble of background/analysis are run at the same model resolution (currently TQ0062L028). As a consequence, a recentering of the ensemble mean around the hybrid analysis, is not made. Another point to mention is the fact that the bias mass and angle of the radiance channels and instruments were not being updated. This decision was taken because, as a testing system, no compromise was made to keep the radiance information error updated. Also, there is no vertical localization within the EnSRF, so a fixed value is used for the entire vertical column.

3. Experimental design

To test the hybrid 3DVar system, a set of experiments were idealized in order to verify the analysis and forecasts skill (in terms of the Root Mean Square Error - RMSE and the Anomaly Correlation - AC), by comparing them with a pure (control) 3DVar analysis. The pure 3DVar analysis, in turn, was compared to an offline analysis experiment by integrating the BAMv0 model

with an independent analysis. The next subsection are dedicated to explain the design of each experiment.

a. Control Experiment

The control experiment is intended to be a 3DVar experiment run with the new background error covariance matrix. This experiment is the control run and is compared to the hybrid 3DVar experiments. The control was ran using the variational analysis in TQ0062L028 resolution and the model configuration (both the dynamics and the physics) is the same among every experiment. The analysis cycle is setup in the following manner. A set of three background forecasts of 3, 6 and 9 hours (where the central analysis is always at 6 hours) are used by GSI for the update with the observations in a First Guess at Appropriate Time (FGAT) approach. Observations include conventional data (u, v, T, q and ps) from several sources (e.g., the Global Telecommunication System - GTS) and unconventional data, like radiance, retrievals and Global Positioning System - Radio Occultation (GPS-RO).

Table 2 in Section 3c summarizes the types of observations included in the experiments. The same set of observations are used for the hybrid 3DVar experiments as well.

The analysis cycles continues when GSI writes the analysis file for the atmosphere and the surface. It is worth to note that only the atmospheric part of the analysis was used to initialize the BAMv0, although the model restart files were used to initialize the surface fields, as well clouds and radiation. This same approach is taken for the hybrid experiments.

Another idealized experiment is the offline analysis (i.e., without an analysis cycle). In this experiment the BAMv0 where integrated in time with a hi-resolution NCEP spectral operational analysis which was chopped at each analysis time (i.e., 00, 06, 12 and 18UTC). From this experiment, 120 hours forecasts are generated, in the same fashion as the pure 3DVar run. This

offline experiment is intended to serve as a control for the pure 3DVar experiment, whereas the pure 3DVar analysis experiment serves as a control for the hybrid 3DVar experiments.

b. Hybrid 3DVar Experiments

Exercising with the hybrid 3DVar was made cycling the system with the BAMv0 model between December 2012 and January 2013. A spin up time was considered and the first month of the simulations was taken apart from the results. One of the reasons for this practice is the fact that the initial ensemble of analysis was generated by running the BAMv0 model from a single deterministic analysis and forecasts made up to 30 days at each 12 hours (i.e., twice a day). From this, a time series of 60 forecasts ranging from 12 hours up to 720 hours from the analysis time was assembled. The first 40 forecasts were kept and carefully modified to reflect the background time for the first analysis to be generated in all hybrid 3DVar experiments.

To assess the behaviour of the hybrid 3DVar system using the BAMv0 model as a background and its new background error covariance matrix, two cycled data assimilation experiments were ran. The experiment called 3DVar represents the variational GSI/3DVar experiment with the new **B** (considering $\alpha_1 = 1$, i.e., no ensemble covariance contribution). The experiment called EnSRF50 (EnSRF75) represent the same data assimilation cycle ran using the hybrid **B** through the use of the EnSRF (considering $\alpha_2 = 0.5$ and $\alpha_2 = 0.25$, i.e., considering 50% and 75% of contribution of the ensemble covariances, respectively).

Table 1 summarizes the experiments designed to exercise the hybrid 3DVar system, ranking the ensemble covariance contribution for each experiment.

c. Observational Data

The observational data used for the experiments with a cycled analysis using the 3DVar GSI and the EnSRF algorithm, are the same. Table 2 shows a summary of the observational data used.

d. Model Setup

In all experiments, regardless the analysis used, the same model configuration had been taken. Table 3 summarizes the main options adjusted within the dynamical core and physics options. It is worth to note that in the data assimilation cycle (regardless the hybrid or the pure variational option), the atmospheric model was restarted at every cycle (00, 06, 12 and 18UTC). The BAMv0 restart files comprises the previous states of the land-surface, clouds and radiation. Sea surface temperature, snow cover and soil moisture are read from separated files and the dynamical state (i.e., momentum) are provided by the atmospheric analysis. These conditions are valid for the generation of the background files (3h, 6 and 9 hours forecasts) used by the GSI.

e. GSI Setup

This subsection is intended to give an overview of the basic and main GSI options that was chosen to complete the experimental design. GSI has many different option that can be adjusted in order to allow the system run with specific procedures or to tune the system through the use of knobs that must be adjusted empirically. All of these option can be found on the official GSI manual, available at the Development Testbed Center (DTC) website.

Two of these general options worth to mention here (the choice for humidity control variable and the moisture constraint), as they were kept the same among all experiments using GSI.

Humidity Control Variable

GSI has two options to treat the humidity control variable. They are the pseudo relative-humidity and the normalized relative humidity. As we were testing a new background error covariance matrix, we decided to choose the normalized relative humidity as the humidity control variable in all experiments. The normalized relative humidity allows the relative humidity to change in the inner loops in accordance to changes in the surface pressure, temperature or specific humidity.

Moisture Constraint

Supersaturated and negative moisture are non-physical solutions that arises from computation modes. In GSI, there is an option that can be tuned in order to control the supersaturated and negative moisture. Several tests were made in order to achieve reasonable values to allow the stability of the system. The values found are 5.0 for the supersaturated moisture constraint and 0.005 for the negative moisture constraint.

4. Results

This section shows the results obtained with the application of a hybrid background error covariance matrix through the use of a hybrid 3DVar system for the BAMv0 model. Along with the experimental results, the main characteristics of the calculated background error covariance matrix are shown. Results from the experiments with the hybrid 3DVar are divided into three categories: 1) the ensemble innovation statistics; 2) forecasts skill (up to 120 hours, taken in terms of AC along with t-Student tests) and 3) precipitation assessment (taken in term of a comparison with the GPCP data). The evaluations are made to the regions Global (GL), North Hemisphere (NH - lons:0°-360°; lats:20°N-80°N), Tropics (TR - lons:0°-360°; lats:20°S-20°N), South Hemisphere (SH - lons:0°-360°; lats:80°S-20°S) and South America (SA - lons:0°-360°; lats:49.875°S-11.375°N).

a. Standard Deviations of the Static **B**

Experiments with a cycled data assimilation (analysis from 3DVar and hybrid 3DVar experiments) were made using the same version of the static background error covariance matrix. In Section 2a, it was showed how the static part of the hybrid background error covariance matrix was calculated and how its application within GSI is made. Following the results in Wu et al. (2002), the main features of the static **B** are presented here in a similar manner.

In order to make an quantitative and a qualitative description of the amplitudes represented by the computed covariance matrix, Figure 2 depicts the standard deviations of the variance error for the ψ, χ, T, *rh*, *oz* and *ps*. As a reference, Table 4 presents the maxima and minima values for the amplitudes shown in Figure 2 along with the values for the horizontal and vertical length-scales.

The distribution of the variances of stream function (ψ) and velocity potential (χ) are presented in a vertical cross-section, as shown in Figure 2. These distribution shows some of the features of the non-divergent and divergent part of the wind for the BAMv0 model. The ψ variances distribution are sort of symmetric with respect to the Equator line. They are more elongated throughout the vertical column and are concentrated at the model top. Higher values of the streamfunction variances are located over the poles, between sigma levels of 0.6 ($\sim$614.4 hPa) and 0.2 ($\sim$204.8 hPa). In the tropical regional, these values are more confined between 0.3 ($\sim$307.2 hPa) and 0.1 ($\sim$102.4 hPa) sigma levels. The distribution of the variances of the velocity potential also shows a symmetric pattern with respect to the Equator line and are mostly concentrated with higher values over the tropical region, between sigma levels of 0.3 ($\sim$307.2 hPa) and 0.1 ($\sim$102.4 hPa).

Temperature (T) variances are distribute from the Equator line towards the pole, in both hemispheres. At 30°N large values extend onwards with a maximum peak between 0.9 ($\sim$921.6 hPa) and 0.8 ($\sim$819.2 hPa) sigma layers. At 60°S, a symmetric pattern is represented, as can be seen

in Figure 4c in Wu et al. (2002). Variances of the humidity (*rh*) are distributed with a peak in approximately 60°S between 0.7 (∼716.8 hPa) and 0.6 (∼614.4 hPa) sigma layers. Layers above 0.6 sigma, variances diminish with height until layer 0.2 (∼204.8 hPa), whereas the opposite pattern seems to happen around latitude 60°N. Ozone (*oz*) distribution of variances are concentrated in upper layers, 0.5 (∼512 hPa) upwards, with a peak in the tropical region. In the current setup, GSI does not analyses ozone observations. In the BAMv0 model ozone is transported throughout the grid during the forecast. The surface pressure (*ps*) variances are distributed with two local maxima values in the midlatitudes (higher values are located below 60°S) and minimum values in the tropical region. It is worth to note that the surface pressure variance distribution are fairly different from what can be found in Figure 4e from Wu et al. (2002).

Most of the characteristics in the distribution of the error amplitudes may be due to the representation of the BAMv0 topography, including the choices for the model physics and the treatment of the model dynamics and resolution. At this resolution (i.e., TQ0062L028), steep topography may be not well represented (peaks in topography may be too smooth), what can lead to discrepancies in the representation of the pressure and winds. A separated study still has to be made in order to address the sensitivity of the background error covariance matrix to the BAMv0 options and the resulting variances. Furthermore, one may consider the fact that such amplitudes can be tuned within GSI by setting up specific parameters for the application of the covariances using recursive filters.

Table 4 summarizes the maximum and minimum values for the amplitudes of the standard deviations and horizontal and vertical length-scales, including for the other quantities not shown in Figure 2.

b. Ensemble Innovation Statistics

For an evaluation of the ensemble of analyses produced in experiments using the EnSRF, an ensemble innovation assessment was made in terms of a scaled bias to diagnose deficiencies in the ensemble spread due to inflation and localization adjustment.

To assess how the ensemble deals with the system spread in the presence of observational error, innovations are shown as a measure of how good the ensemble spread is due to the observation innovation. In Figure 3, a comparison between the innovation statistics from EnSRF is shown for three different regions (NH; TR and SH) and only for the conventional observations. We left the same evaluation regarding unconventional observations for a separated study. In order to make it easier to understand, the y axis shows the ratio between the standard deviation of the prior innovations (i.e., $y^o - \mathbf{H}x_k^b$, where k is an ensemble member) and the square root of the ensemble total spread (i.e., $\sqrt{\mathbf{S}+\mathbf{R}}$). The ensemble innovation is given by,

$$EI = \frac{y^o - \mathbf{H}x_k^b}{\sqrt{\mathbf{S}+\mathbf{R}}} \tag{4}$$

where,

- y^o: is the observation vector;
- x_k^b: is the vector of the k-th ensemble member;
- $\mathbf{S}$: is the ensemble spread;
- $\mathbf{R}$: is the observation error from the observation error covariance matrix.

As we are normalizing the standard deviation of the priors innovations by the ensemble total spread, the lower the values, the better the ensemble innovation is. Ideally, the standard devi-

ation of the priors should match the value of the ensemble total spread if the ensemble is well conditioned, i.e., with a good amount of spread and proper localization and inflation.

In Figure 3, the upper panel shows the statistics for 00UTC and the bottom panel the same statistics for 12UTC. This was made with the purpose to reduce the size of the time series and to separate the signal from both times, so this would make easier to analyze the results. Furthermore, synoptic times of 06 and 18UTC were kept away from the evaluation due to the fact that there is less meteorological observations at these synoptic times. Red lines (dashed and solid) refers to the hybrid 3DVar experiment where 50% of ensemble contribution to the static part of the covariance matrix, whereas the blue lines refers to the same experiment but denoting the case where 75% of ensemble contribution to the static part of the covariances were drawn.

Figures 3d,e,f (in both panels) with the ensemble innovation statistics for T at NH, TR and SH, regardless the relative amount of ensemble contribution, shows that the differences between the priors and the posteriors are more noticeable at the NH, where T is closer to the zero line.

The standard deviation for the horizontal wind (uv) at 00UTC (Figure 3a), was very close to the ensemble total spread, indicating that the ensemble fit to the observation was good and the amount of ensemble spread was reasonable. At the TR region (Figure 3b), however, the opposite was found. In the SH region (Figure 3c), a similar situation to NH happens and the amplitude of the ensemble innovation signal increases indicating, possibly, that the lack of ensemble inflation due to reduced number of conventional observation in the region. Innovation statistics for variables q follows the trends figured for T, with increasing values over TR regions all along the simulations. For the surface pressure, on the other hand, innovation statistics seems to decrease with time (in both 00 and 12UTC), specially over SH region. This may be an indication that the ensemble spread is not good there.

c. Forecast Skill

The forecast skill up to 5 days, was assessed in terms of the Anomaly Correlation (AC). As CPTEC developments are focused in the Tropics and the the South America regions, results are shown for these region along with for the whole Globe and North and South Hemispheres. To assess how different the experiments are between each other, a t-Student test was also made with a 95% of confidence level. For each plot of the AC, a t-Student test is presented and the lower boxes shows whether or not the curves are different at the defined confidence level. When the curves crosses their respective boxes, it means that the differences between the experiment (e.g., EnSRF50) and the experiment of reference (i.e., REF, the BAMv0 model integrated with the operational NCEP analysis) are of no difference, indicating that the test for the null hypothesis fails. In this case, the null hypothesis is that the mean of the hybrid experiment verified is statistically indistinguishable from the mean of the experiment of reference.

Figure 4 shows the 5-day forecasts AC with a t-Student test for regions NH, TR and SH. Figure 5 shows the 5-day forecasts AC with the same t-Student test, but for the regions GL and SA. Variables evaluated are the surface pressure (*psnm*), specific humidity at 925 hPa ($q925$), air temperature at 850 hPa ($T850$), zonal wind component at 250 hPa ($u250$) and geopotential height at 500 hPa ($z500$). Experiments summarized in Table 1 were run with the same configuration (i.e., using the same code and options chosen through namelists).

Experiment EnSRF50 indicate the best analysis performance for all regions and variables evaluated. Surface pressure (*psnm*) at NH has practically no difference using either EnSRF75 or EnSRF50 for the first 24 hours of forecasts.

In the TR region - a region specially difficult to predict for, forecast of *psnm*, $q925$ and $T850$ (Figures 4b,e,h) from EnSRF75 have shown a good performance with respect to experiments REF

and 3DVar. The improvements with respect to REF for *psnm* (Figure 4b), are of almost 24 hours (considering 80% of the AC). Figure 4e, shows improvements of the experiment EnSRF75 with respect to experiment 3DVar, in the order of almost 4 days in advance (considering 85% of the AC). A similar improvement was found for the forecast of the $T850$ (Figure 4h), with respect to experiment to experiment 3DVar were experiment EnSRF75 still holds 80% of AC for 72 hours forecast, whereas experiment 3DVar limits its forecast skill for this variable up to 36 hours. The zonal component of the horizontal wind at 850 hPa (u850 - Figures 4n), showed an slighly improvement over the TR region. It is worth to note in Figures 4b,h,q the spin up time that the BAMv0 model took to initialize with the GFS-NCEP analysis. However, this effect was not noticed for every evaluated variable. Figure 4g, for example, indicates that there is no practical difference between the experiments whose AC scores are very similar. The t-Student test, however, reveals that the 3DVar experiment did not fail the null hypothesis test for the 120 hours forecasts, while the remaining of the experiments holds the test up to 36 hours (EnSRF50) and 72 hours (EnSRF75). On the other hand, however, experiment EnSRF75 was statistically different from the REF up to 72 hours.

Figure 5 shows the same evaluation as Figure 4, but for regions GL and SA. The SA region is of great interest for CPTEC because it is Brazil's target forecast region. The same response from experiments EnSRF75 and EnSRF50 were found, indicating that for the SA region, the ensemble covariances can also play an important role in the determination of the forecasts skill. For the GL region, AC scores are similar to what we have found on NH region. Besides that, the AC for $q925$ at GL region (Figure 5c), shows that the forecasts drawn from the EnSRF75 experiment was good up to 120 hours. Remaining variables (i.e., *psnm*, $T850$, $u250$ and $z500$ - Figures 5a,e,g,i, respectively) showed similar AC scores in comparison with the NH region. For the SA region, good results were found *psnm* (Figure 5b), for up to 84 hours forecasts; $q925$ (Figure 5d), with AC greater than 85% for 120 hours and $T850$ (Figure 5f) with AC of 80% from experiment

EnSRF75 for up 72 hours forecasts. Zonal wind at 250 hPa ($u250$) and, specially, $z500$, did not drawn good AC scores. The $z500$ (Figures 5k,l) from experiment EnSRF75 did not performed well as for others variables. From 84 hours forecast ahead, its was the worse and experiment EnSRF50 - and even experiment 3DVar, were better.

A comparison between the analysis schemes used in the experiments, shows that the humidity analysis drawn from the EnSRF50 experiment, was improved over the pure 3DVar analysis. For these hybrid 3DVar experiments, background error covariance matrix is the same static covariance matrix used within the 3DVar experiment. This is an indication that the ensemble covariance plays an important role on defining how the analysis increments are applied.

Precipitation Assessment

Precipitation forecasts drawn from the REF experiment and from the pure 3DVar and the hybrid 3DVar analysis has been also evaluated. Figure 6a shows the observed Global Precipitation Climatology Project v2.2 (GPCPv2.2) 2.5° (Adler et al. 2003) global monthly mean precipitation and the forecasted precipitation - represented as a monthly mean, drawn from the REF (Figure 6b), 3DVar (Figure 6c), hybrid 3DVar analyses with EnSRF50 (Figure 6d) and EnSRF75 (Figure 6e). The comparison between the 24 hour monthly mean forecasts and the GPCP 2.5 is valid for January 2013 (12UTC) and the gridded data has been interpolated to a 2.5° grid resolution to match GPCPv2.2. GPCP 24 hour monthly mean precipitation for January 2013 depicts the main features of the tropical precipitation (from 8 mm above) and the subtropical precipitation (until 8 mm), with most of the convective precipitation being distributed over the tropical region.

The precipitation fields being compared in Figure 6a represents the monthly mean at 12UTC beginning at 1st January 2013, until 31rd January 2013. All experiments shows the spatial features of the large scale precipitation and the convective precipitation as well. Figure 6a is used as a

reference and the evaluation is made by comparing the precipitation intensity, distribution and the spatial average of the monthly mean, annotated below each picture.

The precipitation forecasts from the experiments, shows a reasonable spatial distribution in comparison with GPCPv2.2 monthly mean precipitation. It is worth to note that the model configuration for large scale condensation, cumulus convection and horizontal and vertical diffusion were kept the same, so the differences are supposed to be due to the initial condition only. Main differences between precipitation forecasts from experiments are mostly related to the intensity of the precipitation, once the spatial distribution between them are fairly similar. Figure 6b, shows the resulting monthly mean 24 hour precipitation from the BAMv0 model initialized with the REF analysis. In comparison with any other experiment (including the GPCPv2.2 reference), the BAMv0 model tended to produce more convective precipitation in the Tropical region. The spatial average of the time mean amounts to 2.9718 mm/month, yielding the highest value among the experiments, even higher than GPCPv2.2 (2.7197 mm/month). All experiments with data assimilation cycle, on the other hand, have produced precipitation with less concentrated distribution and a more reasonable spatial average. The spatial average in experiment EnSRF50 (Figure 6d) is the one which more approximates GPCPv2.2, although the rest of the data assimilation experiments has concentrated the convective precipitation in a more conformable way.

The exaggerated amount of precipitation produced by experiment REF must be due to fact that this experiment was made by just running the BAMv0 model with the GFS-NCEP analysis, although a topography smoothing and a initialization with normal modes has been made for every analysis used in this specific experiment. The choices for the cumulus parametrization and the diffusion parameters may also play an important role in the precipitation production. The experiments with the data assimilation cycle, with the exception of experiment EnSRF75 (Figure 6e) -

which is the experiment that yielded the lower monthly mean, seems to be well conditioned with the option chosen for the forecasts.

In order to better understand and to identify the regions where the experiments have accumulated more or less the precipitation, Figure 7 shows the time series of the spatial averages for each experiment, including the GPCP. In this figure, the GPCPv1.2 1DD (1 Degree Daily - Huffman et al. 2001) was used and the observed data has been interpolated to the analysis grid (with 1.875°). Accompanying Figure 7, Tables 5 and 6 shows the spatial averages (μ) and the standard deviations (σ) for each experiment (including the interpolated GPCP1DD) at the regions evaluated (GL, NH, TR, SH and SA).

In contrast to what we have found by analyzing the spatial distribution of the precipitation forecasts in Figure 6, the time series for the spatial averages showed in Figure 7, shows us that - with the exception of region NH (Figure 7b), all experiments have some difficulties to reproduce the observed precipitation in 24 hour forecasts. Deficiencies can be noted with respect to the amplitude (maxima and minima) and to the average. In some specific cases, forecasted precipitation nearly matched observed values - e.g., experiment EnSRF75 in TR region (Figure 7c) which matched the GPCPv1.2 during some periods of the month. This results is with accordance to what we found when analyzing the forecast skill (Figures 4 and 5), showing that among the hybrid 3DVar experiments, the 75% of the EnSRF ensemble contribution to the static part of the background error covariance was beneficial in most cases. On the other hand, experiment REF have exaggerated the precipitation over time mainly for the GL and TR regions (Figures 7a and 7c). This is an expected result, since this experiment have used an independent analysis and the model was not configured to give the best result from it. For the TR and SA regions (Figures 7c,e), precipitation forecasts were mostly above the observed values indicated by GPCPv1.2. In these regions, the convective precipitation plays an important role and models tend to exaggerate the precipitation there. If we

consider the SH region (Figure 7d) - which contains more oceanic parts (in opposition to the NH region), models tends to produce more large-scale precipitation whereas the convective precipitation tends to be less important in the results. Consequently, the precipitation forecasts tends to be below the observed values.

All experiments with the hybrid background error covariance matrix showed reasonable results if compared to experiments 3DVar and REF. It appears, however, that the precipitation - specially the convective precipitation, to be not so sensitive to changes in the covariance matrix, although the experiment with greater ensemble contributions (EnSRF75) do perform better than the rest of the experiments made.

5. Summary and discussion

In this work we have tested an implementation of the hybrid 3D variational (hybrid 3DVar) data assimilation technique with the BAMv0 model. For this implementation, we carried out the calculation of a static background error covariance matrix used in the linear combination with the covariances from the ensemble part. To test the implementation, experiments were made in a TQ0062L028 model and analysis resolution using an ensemble of analysis of 40 members, testing the EnSRF algorithm. Results shows an general improvement of the winds, temperature, moisture and surface pressure, mainly over South America and the Tropical region, which is a target region for CPTEC operations. The moist part of the BAMv0 model (e.g., Specific Moisture, Precipitable Water and Precipitation) resulted in a slight difference from the control run (the BAMv0 model initialized with the GFS-NCEP analysis) and the from the BAMv0 model simulation initialized with the pure 3DVar analysis.

In this work it is clear that the ensemble contributions to the static part of the covariance matrix plays an important role in determining the skill of the analysis, and consequently the skill of the

forecasts. In some cases, we found improvements of more than 3 days, which we consider a great step towards a robust analysis to use in daily operations. Furthermore, with this implementation, we could not only show that our implementation is in the right way, but also that we could improve the pure 3DVar analysis (despite some practical issues that have to be properly addressed). Our results corroborates and contribute to the understanding of the application of hybrid background error covariances matrices.

Further improvements to this work shall include the treatment of the caveats pointed out in Section 2c. The realization of the hybrid 3DVar system at CPTEC operations will also depends on the CPTEC capacity to keep the system at a higher resolution without compromise the system performance and to afford the computational cost involved. A study regarding the dual resolution feature for the hybrid system must be considered as the resolution of the ensemble limits the system performance, and the use of the re-centering and ensemble inflation.

Acknowledgments. The authors are thankful to Ricardo Todling for the guidance and multiple discussions during the implementation of the hybrid 3DVar system at CPTEC. The authors are also thankful to the CPTEC staff and to the anonymous reviewers for the corrections and the suggestions that improved the manuscript. To CAPES for the financial support in the PDSE program (grant number BEX 99999.008036/2014-04).

References

Adler, R. F., and Coauthors, 2003: The Version–2 Global Precipitation Climatology Project (GPCP) Monthly Precipitation Analysis (1979–Present). *Journal of Hydrometeorology*, **4 (6)**, 1147–1167, doi:10.1175/1525-7541(2003)004⟨1147:TVGPCP⟩2.0.CO;2, URL http://dx.doi.org/10.1175/1525-7541(2003)004⟨1147:TVGPCP⟩2.0.CO;2, http://dx.doi.org/10.1175/1525-7541(2003)004⟨1147:TVGPCP⟩2.0.CO;2.

Berre, L., M. Monteiro, and C. Pires, 2013: An Impact Study of Updating Background Error Covariances in the ALADIN-France Data Assimilation System. *Journal of Geophysical Research: Atmospheres*, **118 (19)**, 11,075–11,086, doi:10.1002/jgrd.50847, URL http://dx.doi.org/10.1002/jgrd.50847.

Cavalcanti, I. F. d. A., and Coauthors, 2002: Global Climatological Features in a Simulation using the CPTEC-COLA AGCM. *Journal of Climate*, **15 (21)**, 2965–2988, URL http://urlib.net/sid.inpe.br/iris@1915/2005/05.05.11.19.

Chou, M., 1999: *A Solar Radiation Parameterization for Atmospheric Studies.* NASA technical memorandum, URL https://books.google.com.br/books?id=_gYbvgAACAAJ.

Clayton, A. M., A. C. Lorenc, and D. M. Barker, 2013: Operational Implementation of a Hybrid Ensemble/4D–Var Global Data Assimilation System at the Met Office. *Quarterly Journal of the Royal Meteorological Society*, **139 (675)**, 1445–1461, doi:10.1002/qj.2054, URL http://dx.doi.org/10.1002/qj.2054.

Corazza, M., and Coauthors, 2003: Use of the Breeding Technique to Estimate the Structure of the Analysis "errors of the day". *Nonlinear Processes in Geophysics*, **10 (3)**, 233–243, doi:10.5194/npg-10-233-2003, URL http://www.nonlin-processes-geophys.net/10/233/2003/.

Cunningham, C., B. J. P., and M. Ferreira, 2015: Assessing Improved CPTEC Probabilistic Forecasts on Medium-Range Timescale. *Meteorological Applications*, **22 (3)**, 378–384, doi:10.1002/met.1464, URL http://dx.doi.org/10.1002/met.1464.

Desroziers, G., 1997: A Coordinate Change for Data Assimilation in Spherical Geometry of Frontal Structures. *Monthly Weather Review*, **125 (11)**, 3030–3038, doi:10.1175/1520-0493(1997)125⟨3030:ACCFDA⟩2.0.CO;2, URL http://dx.doi.org/10.1175/

591 1520-0493(1997)125⟨3030:ACCFDA⟩2.0.CO;2, http://dx.doi.org/10.1175/1520-0493(1997)
592 125⟨3030:ACCFDA⟩2.0.CO;2.

593 Figueroa, S. N., and Coauthors, 2016: The Brazilian Global Atmospheric Model (BAM):
594 Performance for Tropical Rainfall Forecasting and Sensitivity to Convective Scheme
595 and Horizontal Resolution. *Weather and Forecasting*, **31 (5)**, 1547–1572, doi:10.1175/
596 WAF-D-16-0062.1, URL http://dx.doi.org/10.1175/WAF-D-16-0062.1, http://dx.doi.org/10.
597 1175/WAF-D-16-0062.1.

598 Fisher, M., 2003: Background Error Covariance Modelling. *Seminar on Recent Developments in*
599 *Data Assimilation for Atmosphere and Ocean, 8-12 September 2003*, ECMWF, Shinfield Park,
600 Reading, ECMWF, 45-64.

601 Grell, G. A., 1993: Prognostic Evaluation of Assumptions Used by Cumulus Parameteriza-
602 tions. *Monthly Weather Review*, **121 (3)**, 764–787, doi:10.1175/1520-0493(1993)121⟨0764:
603 PEOAUB⟩2.0.CO;2, URL http://dx.doi.org/10.1175/1520-0493(1993)121⟨0764:PEOAUB⟩2.0.
604 CO;2, http://dx.doi.org/10.1175/1520-0493(1993)121⟨0764:PEOAUB⟩2.0.CO;2.

605 Hamill, T. M., and C. Snyder, 2000: A Hybrid Ensemble Kalman Filter–3D Variational Anal-
606 ysis Scheme. *Monthly Weather Review*, **128 (8)**, 2905–2919, doi:10.1175/1520-0493(2000)
607 128⟨2905:AHEKFV⟩2.0.CO;2, URL http://dx.doi.org/10.1175/1520-0493(2000)128⟨2905:
608 AHEKFV⟩2.0.CO;2.

609 Harshvardhan, R. Davies, D. A. Randall, and T. G. Corsetti, 1987: A Fast Radiation Param-
610 eterization for Atmospheric Circulation Models. *Journal of Geophysical Research: Atmo-*
611 *spheres*, **92 (D1)**, 1009–1016, doi:10.1029/JD092iD01p01009, URL http://dx.doi.org/10.1029/
612 JD092iD01p01009.

Hayden, C. M., and R. J. Purser, 1995: Recursive Filter Objective Analysis of Meteorological Fields: Applications to NESDIS Operational Processing. *Journal of Applied Meteorology*, **34 (1)**, 3–15, doi:10.1175/1520-0450-34.1.3, URL http://dx.doi.org/10.1175/1520-0450-34.1.3, http://dx.doi.org/10.1175/1520-0450-34.1.3.

Holtslag, A. A. M., and B. A. Boville, 1993: Local Versus Nonlocal Boundary–Layer Diffusion in a Global Climate Model. *Journal of Climate*, **6 (10)**, 1825–1842, doi:10.1175/1520-0442(1993)006⟨1825:LVNBLD⟩2.0.CO;2, URL http://dx.doi.org/10.1175/1520-0442(1993)006⟨1825:LVNBLD⟩2.0.CO;2, http://dx.doi.org/10.1175/1520-0442(1993)006⟨1825:LVNBLD⟩2.0.CO;2.

Huffman, G. J., R. F. Adler, M. M. Morrissey, D. T. Bolvin, S. Curtis, R. Joyce, B. McGavock, and J. Susskind, 2001: Global Precipitation at One-Degree Daily Resolution from Multisatellite Observations. *Journal of Hydrometeorology*, **2 (1)**, 36–50, doi:10.1175/1525-7541(2001)002⟨0036:GPAODD⟩2.0.CO;2, URL http://dx.doi.org/10.1175/1525-7541(2001)002⟨0036:GPAODD⟩2.0.CO;2, http://dx.doi.org/10.1175/1525-7541(2001)002⟨0036:GPAODD⟩2.0.CO;2.

Lorenc, A. C., 1986: Analysis Methods for Numerical Weather Prediction. *Quarterly Journal of the Royal Meteorological Society*, **112 (474)**, 1177–1194, doi:10.1002/qj.49711247414, URL http://dx.doi.org/10.1002/qj.49711247414.

Lorenc, A. C., 2003: Modelling of Error Covariances by 4D–Var Data Assimilation. *Quarterly Journal of the Royal Meteorological Society*, **129 (595)**, 3167–3182, doi:10.1256/qj.02.131, URL http://dx.doi.org/10.1256/qj.02.131.

Mellor, G. L., and T. Yamada, 1974: A Hierarchy of Turbulence Closure Models for Planetary Boundary Layers. *Journal of the Atmospheric Sciences*, **31 (7)**, 1791–1806,

636 doi:10.1175/1520-0469(1974)031⟨1791:AHOTCM⟩2.0.CO;2, URL http://dx.doi.org/10.1175/
637 1520-0469(1974)031⟨1791:AHOTCM⟩2.0.CO;2, http://dx.doi.org/10.1175/1520-0469(1974)
638 031⟨1791:AHOTCM⟩2.0.CO;2.

639 Mendonça, A. M., and J. P. Bonatti, 2009: Experiments with EOF–Based Perturbation Meth-
640 ods and Their Impact on the CPTEC/INPE Ensemble Prediction System. *Monthly Weather*
641 *Review*, **137 (4)**, 1438–1459, doi:10.1175/2008MWR2581.1, URL http://dx.doi.org/10.1175/
642 2008MWR2581.1, http://dx.doi.org/10.1175/2008MWR2581.1.

643 Parrish, D. F., and J. C. Derber, 1992: The National Meteorological Center's Spectral
644 Statistical-Interpolation Analysis System. *Monthly Weather Review*, **120 (8)**, 1747–1763,
645 doi:10.1175/1520-0493(1992)120⟨1747:TNMCSS⟩2.0.CO;2, URL http://dx.doi.org/10.1175/
646 1520-0493(1992)120⟨1747:TNMCSS⟩2.0.CO;2.

647 Purser, R. J., W.-S. Wu, D. F. Parrish, and N. M. Roberts, 2003a: Numerical Aspects of the
648 Application of Recursive Filters to Variational Statistical Analysis. Part I: Spatially Homo-
649 geneous and Isotropic Gaussian Covariances. *Monthly Weather Review*, **131 (8)**, 1524–1535,
650 doi:10.1175//1520-0493(2003)131⟨1524:NAOTAO⟩2.0.CO;2, URL http://dx.doi.org/10.1175/
651 /1520-0493(2003)131⟨1524:NAOTAO⟩2.0.CO;2, http://dx.doi.org/10.1175//1520-0493(2003)
652 131⟨1524:NAOTAO⟩2.0.CO;2.

653 Purser, R. J., W.-S. Wu, D. F. Parrish, and N. M. Roberts, 2003b: Numerical Aspects of the
654 Application of Recursive Filters to Variational Statistical Analysis. Part II: Spatially Inhomo-
655 geneous and Anisotropic General Covariances. *Monthly Weather Review*, **131 (8)**, 1536–1548,
656 doi:10.1175//2543.1, URL http://dx.doi.org/10.1175//2543.1.

Rabier, F., 2005: Overview of Global Data Assimilation Developments in Numerical Weather-Prediction Centres. *Quarterly Journal of the Royal Meteorological Society*, **131 (613)**, 3215–3233, doi:10.1256/qj.05.129, URL http://dx.doi.org/10.1256/qj.05.129.

Riishøjgaard, L. P., 1998: A Direct Way of Specifying Flow-Dependent Background Error Correlations for Meteorological Analysis Systems. *Tellus A*, **50 (1)**, 42–57, doi:10.1034/j.1600-0870.1998.00004.x, URL http://dx.doi.org/10.1034/j.1600-0870.1998.00004.x.

Sellers, P. J., and Coauthors, 1996: A Revised Land Surface Parameterization (SiB2) for Atmospheric GCMs. Part I: Model Formulation. *Journal of Climate*, **9 (4)**, 676–705, doi:10.1175/1520-0442(1996)009⟨0676:ARLSPF⟩2.0.CO;2, URL http://dx.doi.org/10.1175/1520-0442(1996)009⟨0676:ARLSPF⟩2.0.CO;2, http://dx.doi.org/10.1175/1520-0442(1996)009⟨0676:ARLSPF⟩2.0.CO;2.

Thpaut, J.-N., and P. Courtier, 1991: Four-Dimensional Variational Data Assimilation using the Adjoint of a Multilevel Primitive-Equation Model. *Quarterly Journal of the Royal Meteorological Society*, **117 (502)**, 1225–1254, doi:10.1002/qj.49711750206, URL http://dx.doi.org/10.1002/qj.49711750206.

Tiedtke, M., 1983: The Sensitivity of the Time-Mean Large-Scale Flow to Cumulus Convection in the ECMWF Model. *Workshop on Convection in Large-scale Numerical Models, 28 November to 1 December 1983*, ECMWF, Shinfield Park, Reading, ECMWF, 297-316.

Wang, X., 2010: Incorporating Ensemble Covariance in the Gridpoint Statistical Interpolation Variational Minimization: A Mathematical Framework. *Monthly Weather Review*, **138 (7)**, 2990–2995, doi:10.1175/2010MWR3245.1, URL http://dx.doi.org/10.1175/2010MWR3245.1, http://dx.doi.org/10.1175/2010MWR3245.1.

679 Wang, X., D. M. Barker, C. Snyder, and T. M. Hamill, 2008a: A Hybrid ETKF–3DVAR Data
680 Assimilation Scheme for the WRF Model. Part I: Observing System Simulation Experiment.
681 *Monthly Weather Review*, **136 (12)**, 5116–5131, doi:10.1175/2008MWR2444.1, URL http://dx.
682 doi.org/10.1175/2008MWR2444.1.

683 Wang, X., D. M. Barker, C. Snyder, and T. M. Hamill, 2008b: A Hybrid ETKF–3DVAR Data
684 Assimilation Scheme for the WRF Model. Part II: Real Observation Experiments. *Monthly*
685 *Weather Review*, **136 (12)**, 5132–5147, doi:10.1175/2008MWR2445.1, URL http://dx.doi.org/
686 10.1175/2008MWR2445.1.

687 Wang, X., T. M. Hamill, J. S. Whitaker, and C. H. Bishop, 2007: A Comparison of Hybrid Ensem-
688 ble Transform Kalman Filter–Optimum Interpolation and Ensemble Square Root Filter Anal-
689 ysis Schemes. *Monthly Weather Review*, **135 (3)**, 1055–1076, doi:10.1175/MWR3307.1, URL
690 http://dx.doi.org/10.1175/MWR3307.1, http://dx.doi.org/10.1175/MWR3307.1.

691 Wang, X., T. M. Hamill, J. S. Whitaker, and C. H. Bishop, 2009: A Comparison of the Hybrid and
692 EnSRF Analysis Schemes in the Presence of Model Errors due to Unresolved Scales. *Monthly*
693 *Weather Review*, **137 (10)**, 3219–3232, doi:10.1175/2009MWR2923.1, URL http://dx.doi.org/
694 10.1175/2009MWR2923.1, http://dx.doi.org/10.1175/2009MWR2923.1.

695 Wang, X., D. Parrish, D. Kleist, and J. Whitaker, 2013: GSI 3DVar-Based Ensemble-Variational
696 Hybrid Data Assimilation for NCEP Global Forecast System: Single-Resolution Experiments.
697 *Monthly Weather Review*, **141 (11)**, 4098–4117, doi:10.1175/MWR-D-12-00141.1, URL http:
698 //dx.doi.org/10.1175/MWR-D-12-00141.1, http://dx.doi.org/10.1175/MWR-D-12-00141.1.

699 Whitaker, J. S., and T. M. Hammill, 2002: Ensemble Data Assimilation Without
700 Perturbed Observations. *Monthly Weather Review*, **130 (7)**, 1913–1924, doi:10.1175/

1520-0493(2002)130⟨1913:EDAWPO⟩2.0.CO;2, http://dx.doi.org/10.1175/1520-0493(2002)130⟨1913:EDAWPO⟩2.0.CO;2.

Wu, W.-S., R. J. Purser, and D. F. Parrish, 2002: Three-Dimensional Variational Analysis with Spatially Inhomogeneous Covariances. *Monthly Weather Review*, **130 (12)**, 2905–2916, doi:10.1175/1520-0493(2002)130⟨2905:TDVAWS⟩2.0.CO;2, URL http://dx.doi.org/10.1175/1520-0493(2002)130⟨2905:TDVAWS⟩2.0.CO;2, http://dx.doi.org/10.1175/1520-0493(2002)130⟨2905:TDVAWS⟩2.0.CO;2.

Zupanski, M., 2005: Maximum Likelihood Ensemble Filter: Theoretical Aspects. *Monthly Weather Review*, **133 (6)**, 1710–1726, doi:10.1175/MWR2946.1, URL http://dx.doi.org/10.1175/MWR2946.1, http://dx.doi.org/10.1175/MWR2946.1.

LIST OF TABLES

Table 1. Hybrid 3DVar experiments and covariance matrix setup. 36

Table 2. Observational data used in the experiments with a cycled analysis. 37

Table 3. BAMv0 model setup (main options) used within the data assimilation cycles. . . 38

Table 4. Maximum and minimum values of Amplitudes, Horizontal and Vertical Length-Scales of the Static TQ0062L028 background error covariance matrix. . . 39

Table 5. Area average of 24 hour (12UTC) precipitation (in mm/month) for the Globe (GL) and South America (SA). 40

Table 6. Area average of 24 hour (12UTC) precipitation (in mm/month) for the North Hemisphere (NH), Tropics (TR) and South Hemisphere (SH). 41

TABLE 1. Hybrid 3DVar experiments and covariance matrix setup.

Experiment	**Hybrid Setup**	**Description**
REF	–	based on GFS-NCEP
3DVar	–	based on BAMv0-CPTEC
EnSRF50	50% Static/Ens. (40 mem.)	based on BAMv0-CPTEC
EnSRF75	75% Ens. (40 mem.)	based on BAMv0-CPTEC

TABLE 2. Observational data used in the experiments with a cycled analysis.

Mnemonic	**Type**	**Description**
airsbufr	Unconventional	AMSU-A/AIRS radiances from AQUA
amsuabufr	Unconventional	AMSU-A 1b radiances (brightness temperature) from NOAA-15, 16, 17, 18, 19 and METOP-A
hirs4bufr	Unconventional	HIRS4 1b radiances from NOAA 18, 19 and METOP-A
mhsbufr	Unconventional	MHS moisture sounders MHS from NOAA 18, 19 and METOP-A
iasibufr	Unconventional	IASI sounders from METOP-A
gpsrobufr	Conventional	GPS radio occultation refractivities
prepbufr	Conventional	ps, T, q, pw, uv, spd, dw and sst observations

TABLE 3. BAMv0 model setup (main options) used within the data assimilation cycles.

Option	**Setup**
Resolution	TQ0062L028
Integration timestep	1200 seconds
Wind transport	Eulerian
Mass transport	Semi-Lagrangean
Initialization	Diabatic
Restart	Surface
Mass conservation	$ln(p)$
LW radiation	Harshvardhan et al. (1987)
SW radiation	CLiRAD (Chou 1999)
Cumulus convection	Grell (1993)
Shallow convection	Tiedtke (1983)
Top of PBL	Holtslag and Boville (1993)
Bottom of PBL	Mellor and Yamada (1974)
Surface model	SSiB (Sellers et al. 1996)

721 TABLE 4. Maximum and minimum values of Amplitudes, Horizontal and Vertical Length-Scales of the Static

722 TQ0062L028 background error covariance matrix.

	Amplitudes		**Horizontal L-S**		**Vertical L-S**	
	Min	**Max**	**Min**	**Max**	**Min**	**Max**
ψ	$7.60\text{x}10^{5}$	$6.83\text{x}10^{6}$	$4.59\text{x}10^{5}$	$1.31\text{x}10^{6}$	$1.00\text{x}10^{-2}$	$1.48\text{x}10^{0}$
χ	0	$5.05\text{x}10^{6}$	0	$1.95\text{x}10^{6}$	0	$1.60\text{x}10^{0}$
t	0	$2.43\text{x}10^{0}$	0	$7.49\text{x}10^{5}$	0	$1.77\text{x}10^{0}$
q	0	$6.92\text{x}10^{-1}$	0	$7.29\text{x}10^{-1}$	0	$6.61\text{x}10^{5}$
oz	0	$1.76\text{x}10^{6}$	0	$5.90\text{x}10^{5}$	0	$5.30\text{x}10^{0}$
cw	0	$1.95\text{x}10^{6}$	0	$5.00\text{x}10^{5}$	0	$4.91\text{x}10^{0}$
ps	$6.84\text{x}10^{-2}$	$2.29\text{x}10^{-1}$	$3.56\text{x}10^{5}$	$5.26\text{x}10^{5}$	–	–
sst	$2.00\text{x}10^{-2}$	$4.32\text{x}10^{-1}$	$5.07\text{x}10^{2}$	$8.00\text{x}10^{2}$	–	–

723 TABLE 5. Area average of 24 hour (12UTC) precipitation (in mm/month) for the Globe (GL) and South
724 America (SA).

	GL		**SA**	
	μ	σ	μ	σ
GPCP	2.8635	0.1123	3.1321	0.7743
REF	3.0478	0.1036	5.2812	0.7786
3DVar	2.7601	0.1118	5.0152	0.8779
EnSRF50	2.8103	0.0935	4.6480	0.7768
EnSRF75	2.5745	0.1089	3.8128	0.6702

TABLE 6. Area average of 24 hour (12UTC) precipitation (in mm/month) for the North Hemisphere (NH), Tropics (TR) and South Hemisphere (SH).

	NH		**TR**		**SH**	
	μ	σ	μ	σ	μ	σ
GPCP	1.7228	0.2653	4.2820	0.2694	2.6068	0.2053
REF	1.5547	0.2842	5.4655	0.3733	2.0758	0.2685
3DVar	1.4344	0.2438	4.7657	0.3420	2.0499	0.2512
EnSRF50	1.5605	0.2779	4.8385	0.2990	1.9999	0.2546
EnSRF75	1.4566	0.2520	4.2710	0.2209	1.9756	0.2619

LIST OF FIGURES

Fig. 1. Schematic diagram depicting the hybrid 3DVar analysis cycle for the BAMv0 model. 43

Fig. 2. Standard deviations of the variance errors distribution for ψ [10^6 $m^2 s^{-1}$], χ [10^6 $m^2 s^{-1}$], T [K], q, oz and ps [$ln(hPa)$] throughout latitudes and vertical sigma levels. 44

Fig. 3. Ensemble innovation statistics for the EnSRF experiments: red (blue) color represent hybrid analyses with 50% (75%) of EnKF covariances contribution. Upper (bottom) panel plots are valid for 00UTC (12UTC) Dashed lines represents the priors and solid lines represents the posteriors. Left column represent the North Hemisphere (NH), middle the Tropics (TR) and right column, represent the South Hemisphere (SH). 45

Fig. 4. 5-day forecast skill for regions NH, TR and SH. Dashed black line represents the REF experiment analyses and forecasts; solid red line, the 3DVar experiment; magenta line, the EnSRF50 and cyan line, the EnSRF75. All figures are presented with their respective t-Student significance test, where a 95% confidence interval is hold. 46

Fig. 5. Same as Figure 4, but for the GL and SA regions. 47

Fig. 6. Monthly average precipitation 24 hour forecast valid for January 2013 at 12UTC. Comparison is made between monthly mean precipitation from GPCPv2.2 and all experiments using different analyses. In a) GPCP v2.2; b) BAM with the REF analysis; c) BAM with 3DVar; d) BAM with hybrid 3DVar 50% and e) BAM with hybrid 3DVar 75%. Below each picture, it is annotated the spatial average of the monthly mean of the precipitation forecasts, in mm/month. 48

Fig. 7. Spatial averages of the 24 hour forecast precipitation (in mm/day) valid for January 2013 at 12Z. Panel a) precipitation for the whole globe (GL); b) same for the North Hemisphere (NH); c) for Tropics (TR); d) for South Hemisphere (SH) and e) for South America (SA). Precipitation from experiments are compared with the observed precipitation from GPCPv1.2. 49

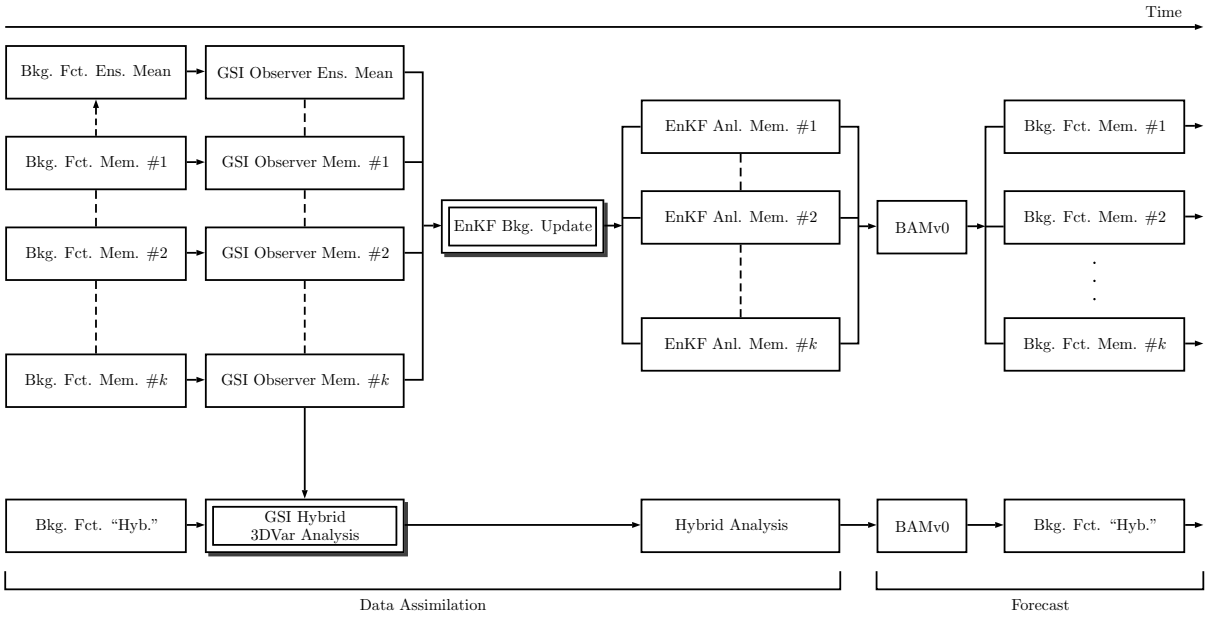

FIG. 1. Schematic diagram depicting the hybrid 3DVar analysis cycle for the BAMv0 model.

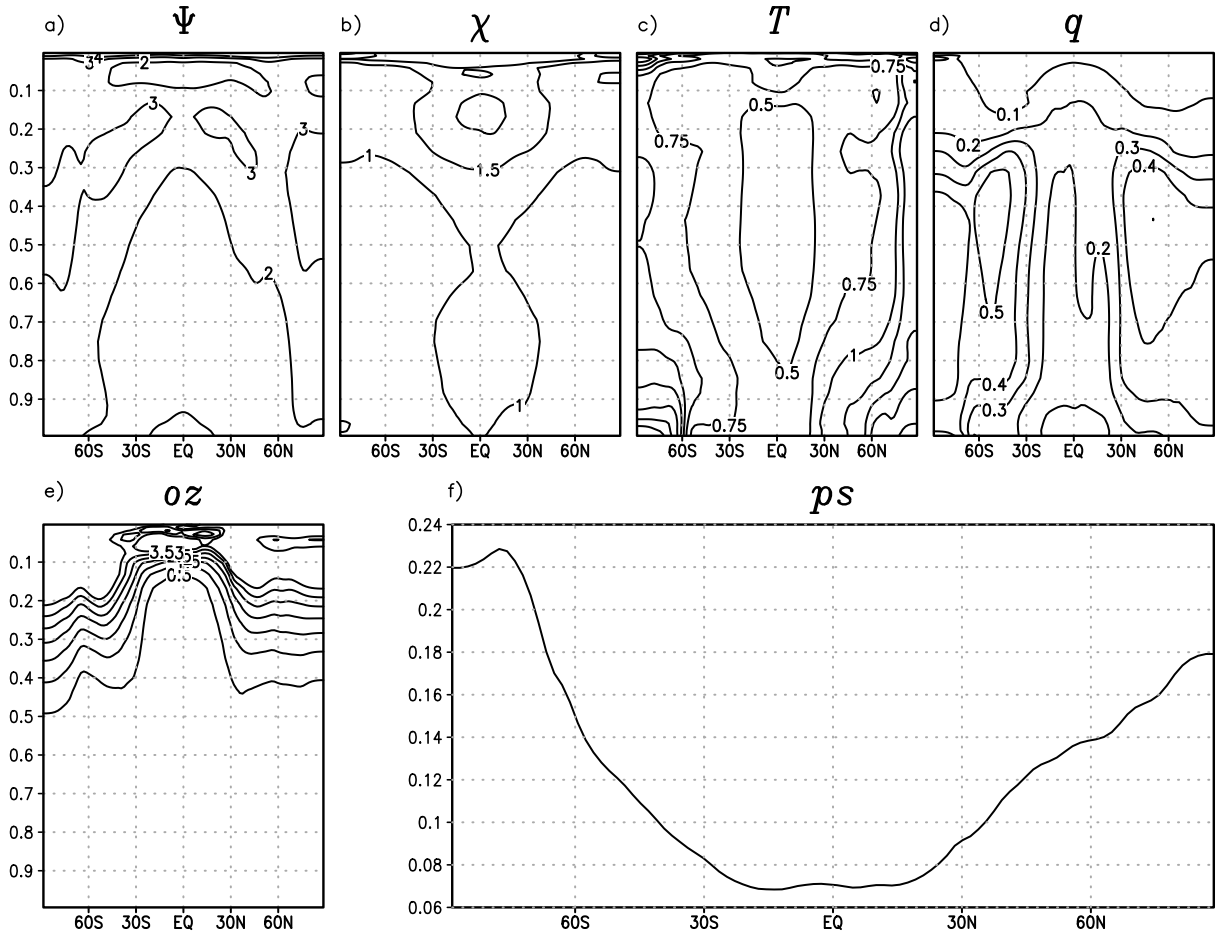

752 FIG. 2. Standard deviations of the variance errors distribution for ψ [$10^6\ m^2 s^{-1}$], χ [$10^6\ m^2 s^{-1}$], T [K], q, oz
753 and ps [$ln(hPa)$] throughout latitudes and vertical sigma levels.

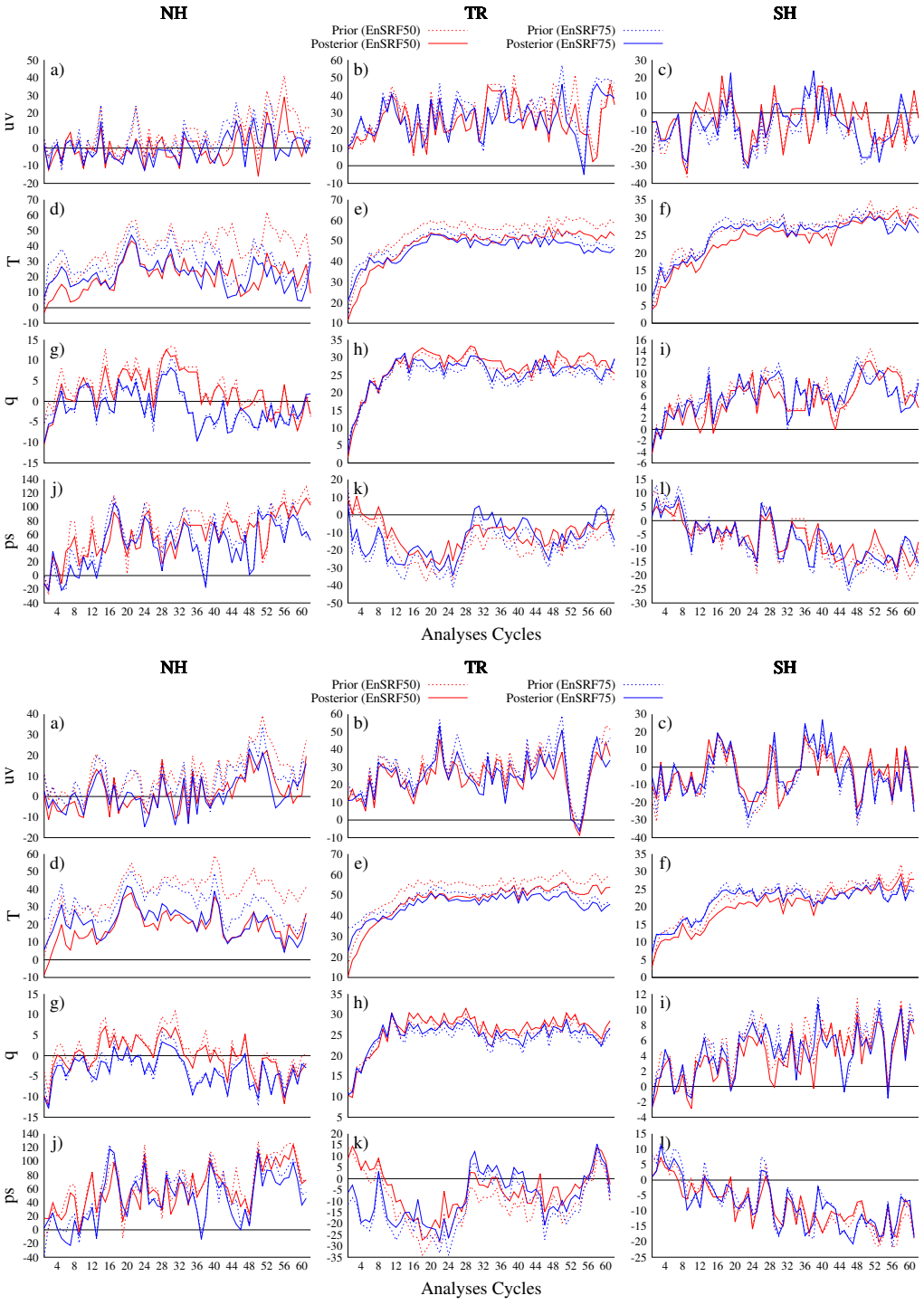

754 FIG. 3. Ensemble innovation statistics for the EnSRF experiments: red (blue) color represent hybrid analyses
755 with 50% (75%) of EnKF covariances contribution. Upper (bottom) panel plots are valid for 00UTC (12UTC)
756 Dashed lines represents the priors and solid lines represents the posteriors. Left column represent the North
757 Hemisphere (NH), middle the Tropics (TR) and right column, represent the South Hemisphere (SH).

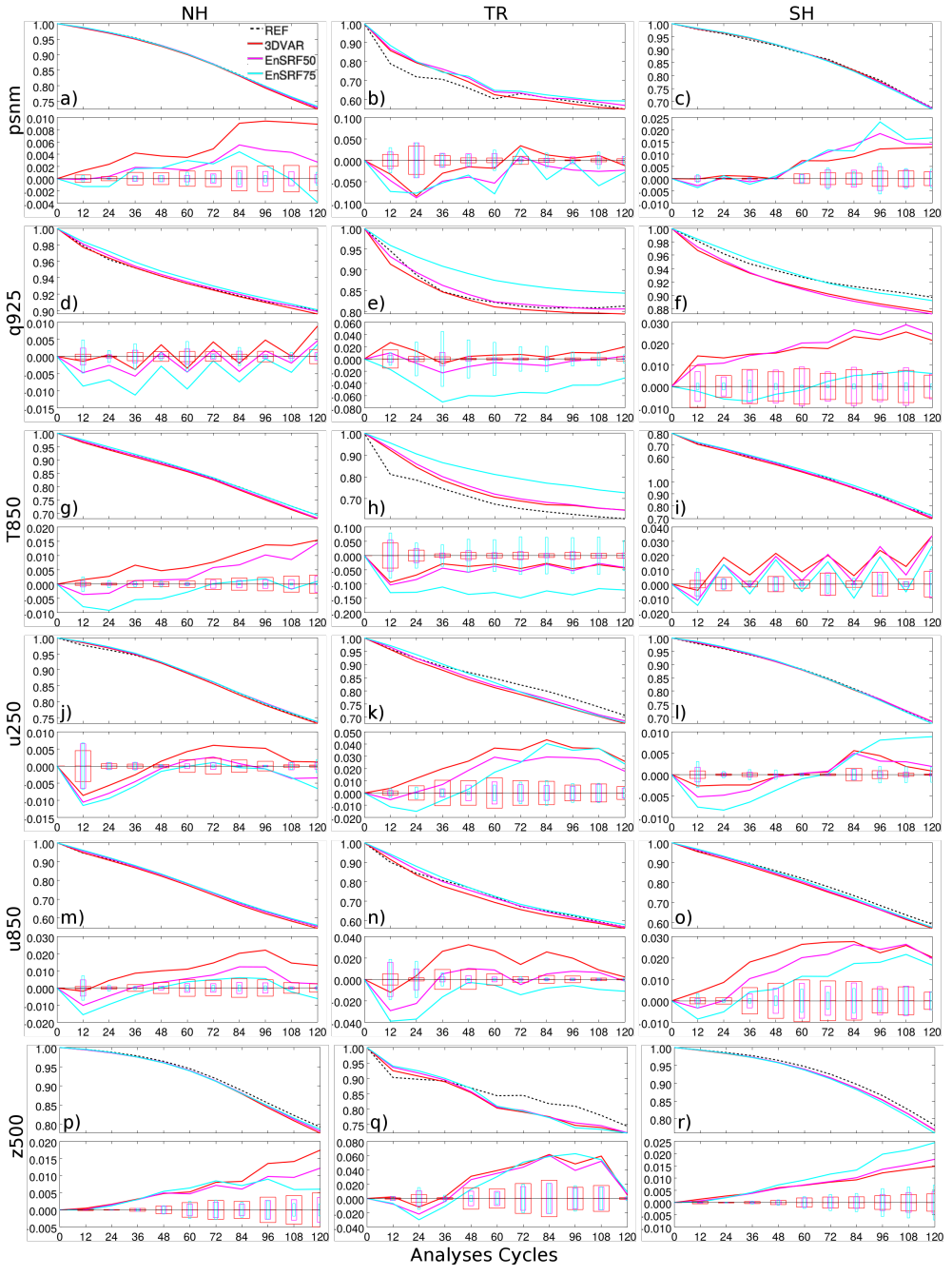

FIG. 4. 5-day forecast skill for regions NH, TR and SH. Dashed black line represents the REF experiment analyses and forecasts; solid red line, the 3DVar experiment; magenta line, the EnSRF50 and cyan line, the EnSRF75. All figures are presented with their respective t-Student significance test, where a 95% confidence interval is hold.

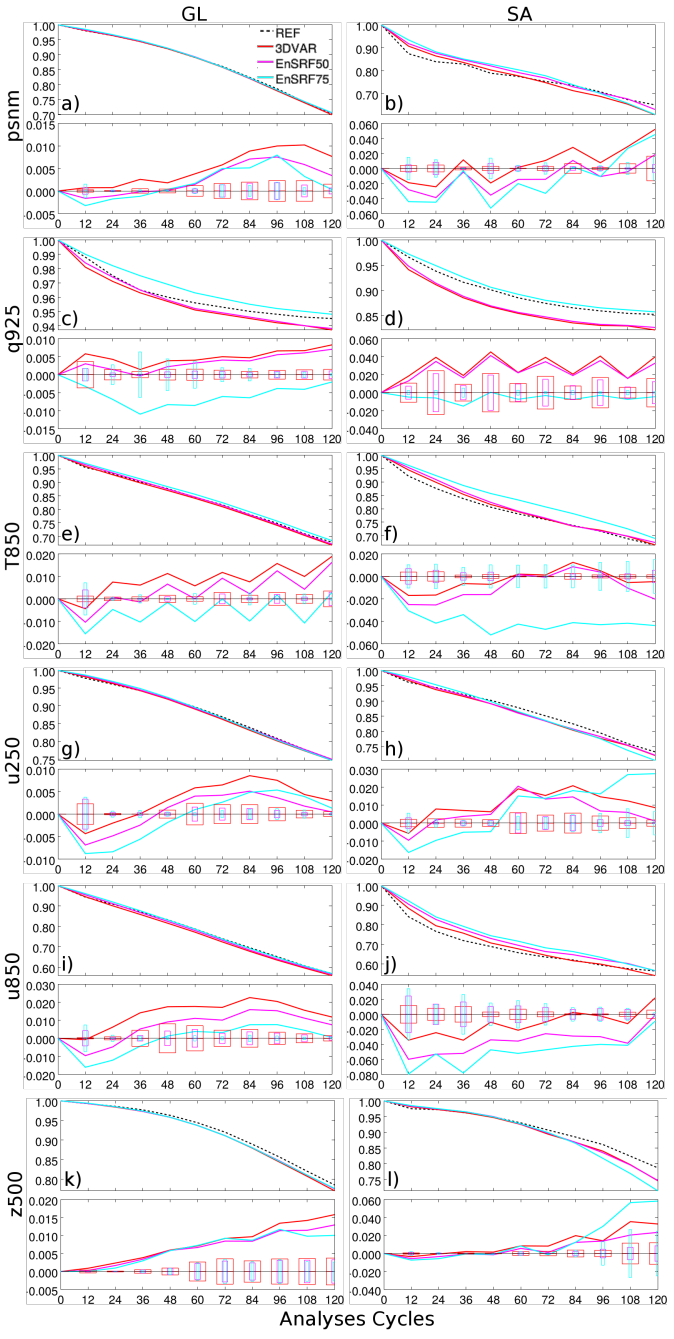

FIG. 5. Same as Figure 4, but for the GL and SA regions.

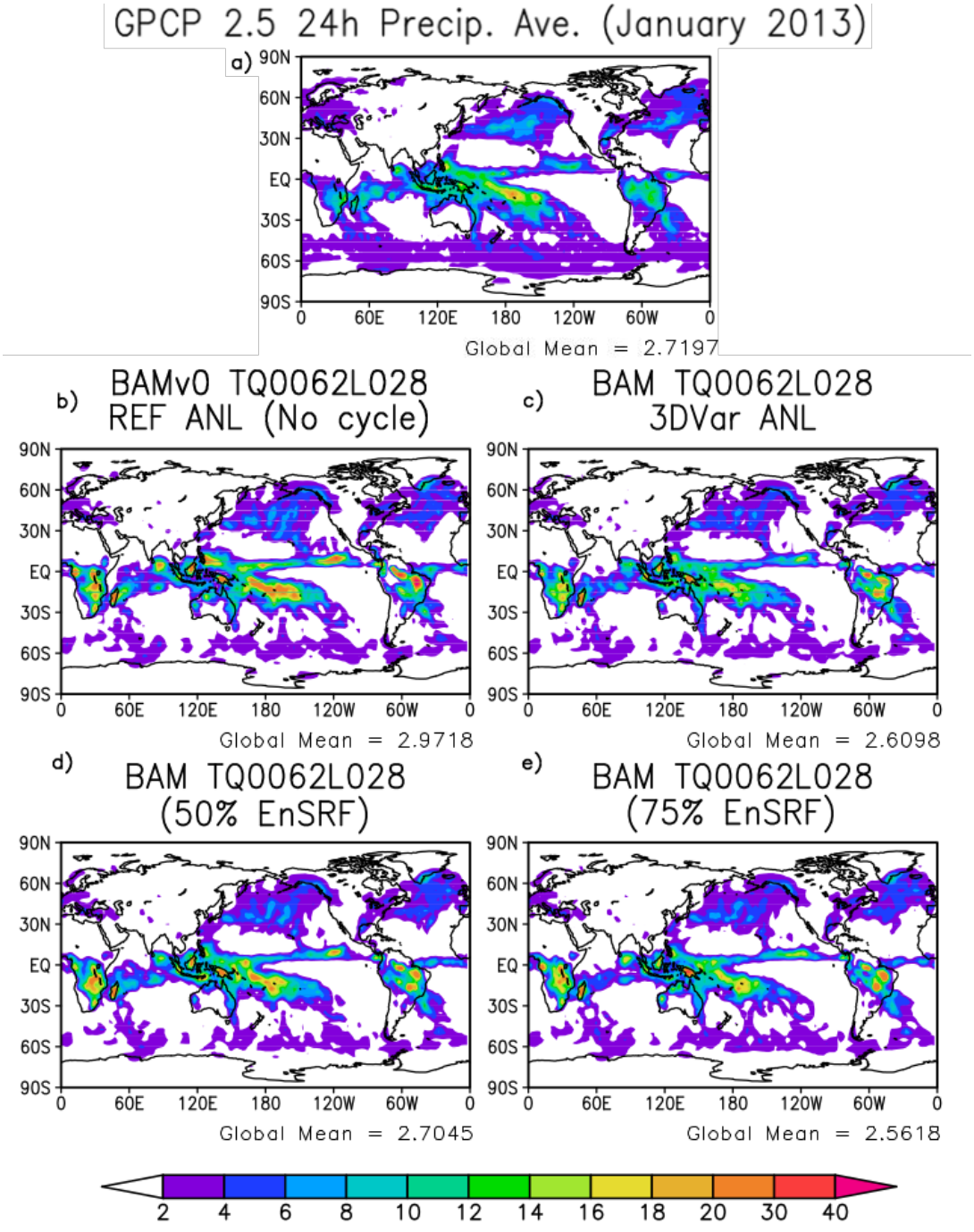

762 FIG. 6. Monthly average precipitation 24 hour forecast valid for January 2013 at 12UTC. Comparison is
763 made between monthly mean precipitation from GPCPv2.2 and all experiments using different analyses. In a)
764 GPCP v2.2; b) BAM with the REF analysis; c) BAM with 3DVar; d) BAM with hybrid 3DVar 50% and e) BAM
765 with hybrid 3DVar 75%. Below each picture, it is annotated the spatial average of the monthly mean of the
766 precipitation forecasts, in mm/month.

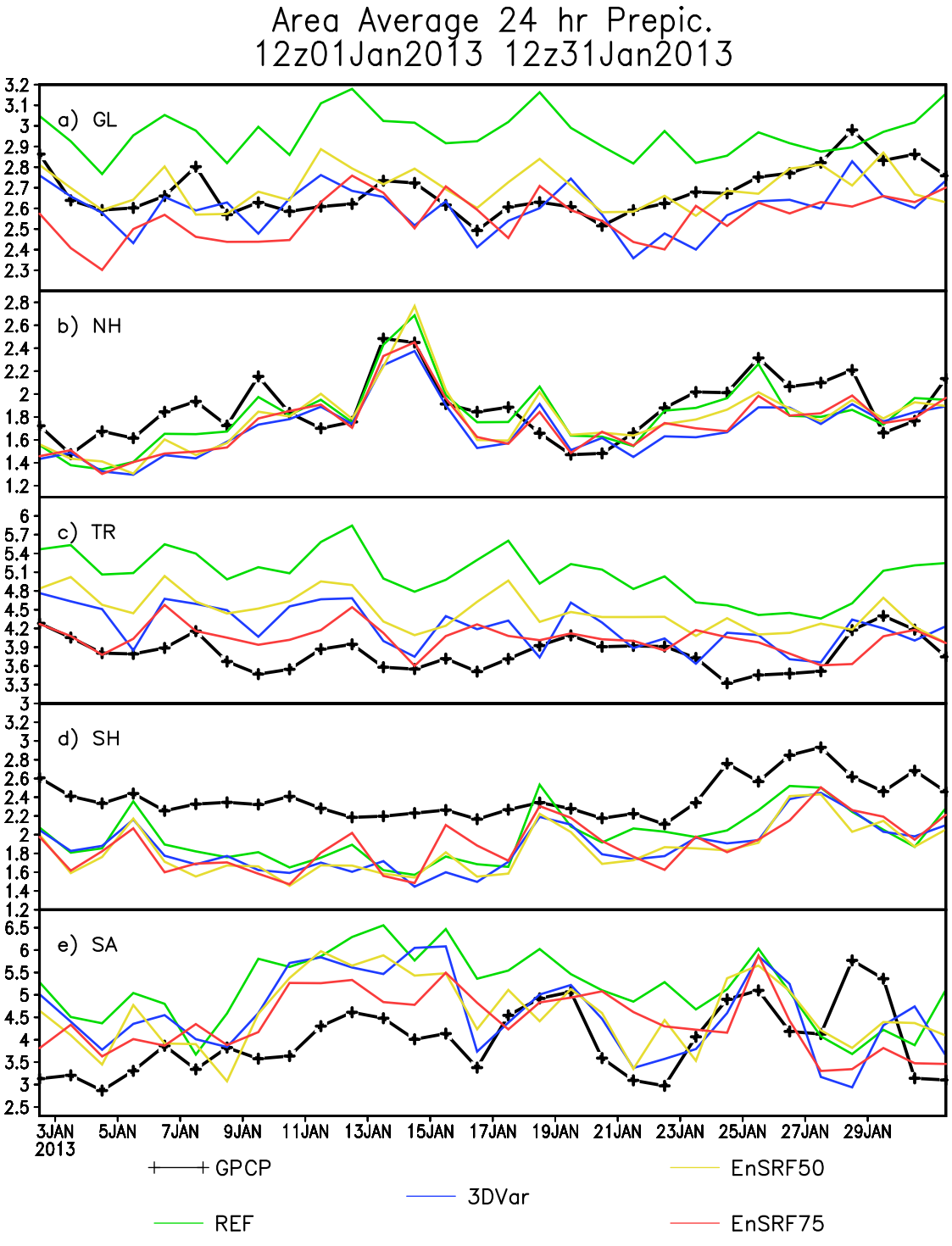

FIG. 7. Spatial averages of the 24 hour forecast precipitation (in mm/day) valid for January 2013 at 12Z. Panel a) precipitation for the whole globe (GL); b) same for the North Hemisphere (NH); c) for Tropics (TR); d) for South Hemisphere (SH) and e) for South America (SA). Precipitation from experiments are compared with the observed precipitation from GPCPv1.2.